Robust Passive Vibration Control of Monopile Offshore Wind Turbines Using a Single-Sided Vibro-Impact Nonlinear Energy Sink Under Wind–Wave–Seismic Loading

Mulatijiang Maimaiti , Ge Yan * , Qunyi Huang , Abudureyimujiang Aosimanjiang , Xiangyu Zhang

Posted Date: 18 May 2026

doi: 10.20944/preprints202605.1085.v1

Keywords: monopile offshore wind turbine; passive vibration control; single-sided vibro-impact nonlinear energy sink; tuned mass damper; wind–wave–seismic loading; frequency detuning; multi-hazard resilience

 doi:10.20944/preprints202605.1085.v1

Article

Robust Passive Vibration Control of Monopile Offshore Wind Turbines Using a Single-Sided Vibro-Impact Nonlinear Energy Sink Under Wind–Wave–Seismic Loading

Mulatijiang Maimaiti [1,2], Ge Yan [1,*], Qunyi Huang [1,3], Abudureyimujiang Aosimanjiang [1] and Xiangyu Zhang [1]

[1] School of Civil Engineering, Kashi University, Kashi 844000, China
[2] Xinjiang Key Laboratory of Engineering Materials and Structural Safety, Kashi 844000, China
[3] School of Civil Engineering, Southwest Jiaotong University, Chengdu 610031, China
* Correspondence: 18971455050@163.com

Abstract

Monopile offshore wind turbines are vulnerable to excessive vibration under coupled wind, wave, and seismic loading because of their slender and flexible structural characteristics. This study investigates a single-sided vibro-impact nonlinear energy sink (SSVI NES) installed inside the nacelle of a 5 MW monopile offshore wind turbine. A reduced-order ten-degree-of-freedom dynamic model is established using the Euler–Lagrange formulation, and turbulent wind, irregular wave, and seismic inputs are generated using TurbSim, the Kaimal and JONSWAP spectra, the Morison equation, and 15 PEER ground motions. The proposed controller is compared with an optimized tuned mass damper (TMD) under nominal and frequency-detuned conditions. The results show that the SSVI NES achieves vibration reduction comparable to that of the optimized TMD under the design condition while requiring a smaller absorber stroke. More importantly, it retains its control effectiveness more stably under frequency detuning, indicating improved robustness against structural-frequency variations. These findings suggest that the SSVI NES is a promising passive solution for enhancing the operational safety and multi-hazard resilience of monopile offshore wind turbines.

Keywords: monopile offshore wind turbine; passive vibration control; single-sided vibro-impact nonlinear energy sink; tuned mass damper; wind–wave–seismic loading; frequency detuning; multi-hazard resilience

1. Introduction

Offshore wind turbines have become an important component of low-carbon energy infrastructure and are increasingly regarded as critical structural assets in the sustainable built environment. Among fixed-bottom support systems, monopile foundations remain one of the most widely adopted solutions in shallow and intermediate water depths because of their structural simplicity, mature installation technology, and cost-effectiveness. However, monopile offshore wind turbines are slender and flexible structural systems with relatively low fundamental frequencies, making them dynamically sensitive to environmental and operational actions. Under routine service conditions, stochastic wind and irregular wave loads act simultaneously on the coupled rotor–tower–foundation system, leading to sustained vibration, fatigue accumulation, and potential serviceability problems. Therefore, vibration mitigation of monopile offshore wind turbines is not only a marine engineering issue, but also an important problem related to the structural safety, serviceability, and resilience of energy infrastructure.

 doi:10.20944/preprints202605.1085.v1

In addition to routine wind–wave excitation, seismic action may become critical for offshore wind turbines located in coastal and seismically active regions. Because monopile-supported offshore wind turbines exhibit low-frequency global modes and significant sensitivity to foundation flexibility, their seismic response may differ substantially from that of conventional fixed-base civil structures. Previous studies have shown that soil–structure interaction, liquefaction, input-motion characteristics, and foundation modeling assumptions can significantly affect the dynamic response and seismic demand of monopile-supported wind turbines. From the perspective of infrastructure resilience, passive vibration-control strategies for offshore wind turbines should therefore be evaluated not only under ordinary wind–wave loading, but also under extreme or accidental seismic disturbances. A multi-hazard assessment framework that considers wind, wave, and seismic actions is essential for understanding the operational safety and long-term robustness of such flexible infrastructure systems.

To suppress excessive vibration, various passive control strategies have been investigated for offshore wind turbines. Among them, tuned mass dampers (TMDs) are the most widely studied because of their simple mechanical configuration, clear design principle, and practical feasibility for nacelle- or tower-mounted installation. Existing studies have demonstrated that single TMDs, multiple TMDs, tuned mass damper inerters, and other modified TMD systems can effectively reduce tower-top displacement, nacelle acceleration, and fatigue-related structural responses under wind–wave, seismic, and combined environmental loading. Recent MDPI studies have also reported TMD-based vibration-control applications for offshore wind turbines and related flexible structures, confirming the continued relevance of passive absorbers in renewable-energy infrastructure. However, the effectiveness of a conventional TMD depends strongly on accurate tuning to the dominant structural frequency. In practical offshore environments, structural frequencies may vary because of scour, soil–structure interaction uncertainty, material degradation, changing operational states, and modeling errors. Once frequency detuning occurs, the performance of linear tuned absorbers may deteriorate significantly. For nacelle-integrated applications, this limitation is not only a control-performance issue but also an implementation issue, because excessive absorber stroke demand may conflict with the restricted internal space and operational layout of the nacelle.

To overcome the narrow-band nature of linear absorbers, nonlinear energy sinks (NESs) have attracted increasing attention in structural dynamics and vibration control. Unlike conventional TMDs, NESs rely on essentially nonlinear restoring behavior rather than precise linear resonance tuning, enabling broadband interaction with the primary structure and promoting targeted energy transfer. Foundational studies have shown that resonance capture, energy pumping, and irreversible energy redistribution are central mechanisms underlying NES behavior. Among different NES configurations, vibro-impact NESs are particularly attractive because intermittent impacts can introduce additional dissipation and enhance nonlinear energy transfer. Single-sided vibro-impact NESs are especially promising for structural control because their unilateral constraint can intensify energy dissipation while limiting the motion of the absorber. These characteristics suggest that an SSVI NES may be suitable for nacelle-mounted vibration mitigation, where robustness and stroke limitation are both important.

Despite these advances, NES-based passive control for offshore wind turbine structures remains much less explored than TMD-based solutions. More importantly, existing studies have not sufficiently clarified whether a single-sided vibro-impact NES can simultaneously satisfy three requirements that are essential for nacelle-mounted control of monopile offshore wind turbines: competitive vibration reduction under nominal multi-hazard loading, reduced absorber motion demand under spatial constraints, and stable retained performance under structural-frequency detuning. This gap limits the practical assessment of impact-assisted nonlinear absorbers for improving the resilience of offshore energy infrastructure.

Motivated by these considerations, this study investigates the robust passive vibration control of a 5 MW monopile offshore wind turbine using a single-sided vibro-impact nonlinear energy sink under combined wind–wave–seismic loading. A reduced-order blade–tower–foundation dynamic

 doi:10.20944/preprints202605.1085.v1

model is developed for repeated time-domain simulations. Turbulent wind fields are generated using TurbSim based on IEC-based wind modeling and the Kaimal spectrum, irregular wave loading is described using the JONSWAP spectrum and Morison equation, and seismic excitation is represented by selected ground-motion records from the PEER database. The proposed SSVI NES is compared with an optimized TMD in terms of nacelle response reduction, absorber motion demand, energy dissipation, and retained control effectiveness under frequency detuning.

The main contributions of this study are threefold. First, a reduced-order dynamic framework is established for comparative assessment of nacelle-mounted passive vibration-control devices under combined wind, wave, and seismic actions. Second, the performance of the proposed SSVI NES is systematically compared with that of an optimized TMD, with particular attention to both structural response reduction and absorber stroke demand. Third, the robustness of the SSVI NES is evaluated under frequency-detuned conditions to clarify its tolerance to off-design structural-frequency variations. Through these contributions, this study aims to provide a practical assessment of SSVI NESs for improving the structural safety, serviceability, and multi-hazard resilience of monopile offshore wind turbines.

2. Numerical Model and Environmental Loading

To evaluate the proposed passive control strategy under realistic multi-hazard conditions, a reduced-order numerical model is established for a monopile offshore wind turbine subjected to combined wind, wave, and seismic excitation. The structural prototype considered in this study is the NREL 5 MW reference offshore wind turbine, which has been widely adopted as a benchmark system for offshore wind turbine dynamics and vibration-control studies [1]. The model is developed to preserve the dominant blade–tower–foundation dynamics while maintaining sufficient computational efficiency for repeated time-domain simulations, parameter studies, and frequency-detuning analysis [4–8].

The external excitations include stochastic turbulent wind, irregular wave loading, and recorded earthquake ground motions. Turbulent wind fields are generated according to IEC-based offshore wind design requirements and the Kaimal spectrum [27,28,31], wave loading is represented using the Morison equation and JONSWAP spectrum [29,30], and seismic excitation is described using ground-motion records selected from the PEER NGA-West2 database [32]. Within this framework, the proposed single-sided vibro-impact nonlinear energy sink (SSVI NES) is assessed against a benchmark tuned mass damper (TMD).

The purpose of the present reduced-order model is not to replace high-fidelity aero-hydro-servo-elastic simulation tools, but to provide a computationally efficient and physically interpretable platform for comparative assessment of passive vibration-control devices. This modeling strategy is particularly suitable for the present study because the evaluation involves repeated simulations under multiple stochastic wind–wave conditions, recorded seismic excitations, and structural-frequency detuning scenarios.

2.1. Coupled Dynamic Model of the Monopile Offshore Wind Turbine

The offshore wind turbine considered in this study is based on the NREL 5 MW reference wind turbine [1]. The structural system consists of a rotor–nacelle assembly mounted on a flexible tower and supported by a monopile foundation embedded in the seabed. To capture the dominant dynamic behavior relevant to vibration-control assessment, a reduced-order ten-degree-of-freedom model is adopted. The retained generalized coordinates include the first flapwise and edgewise modal motions of the three blades, the dominant fore-aft and side-side bending motions of the tower, and the effective translational and rotational motions of the monopile foundation.

As shown in Figure 1, the reduced-order model retains the dominant blade, tower, and foundation motions and includes a nacelle-mounted passive control device. This configuration allows the vibration-control performance of the TMD and the proposed SSVI NES to be evaluated within the same structural framework. The passive control device is assumed to be installed inside

 doi:10.20944/preprints202605.1085.v1

the nacelle and arranged to suppress the tower fore-aft vibration, which is one of the dominant response components under wind–wave and seismic excitation. The TMD provides a linear reference control system, whereas the SSVI NES introduces nonlinear restoring behavior and unilateral impact interaction.

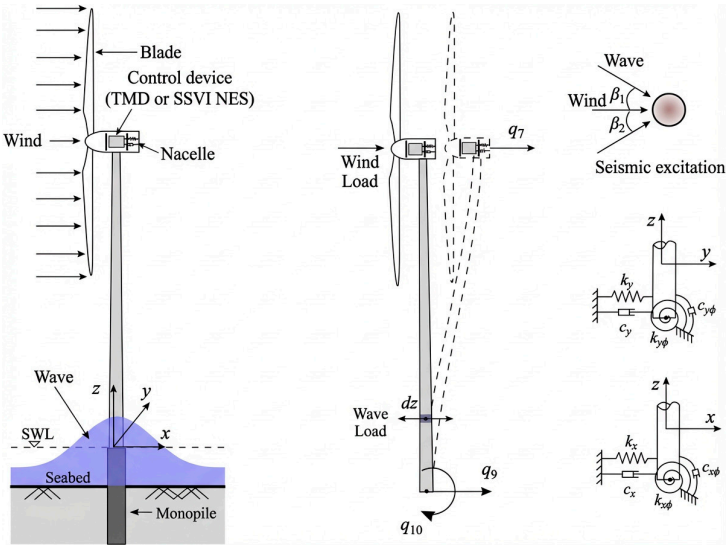

Figure 1. Reduced-order dynamic model of the monopile offshore wind turbine under combined wind, wave, and seismic loading, including the nacelle-mounted passive controller.

To clearly define the retained degrees of freedom, the generalized coordinates adopted in the present 10-DOF model are summarized in Table 1. This reduced-order representation is suitable for repeated time-domain simulations while preserving the dominant blade–tower–foundation dynamics relevant to the assessment of nacelle-mounted passive vibration-control devices.

The generalized displacement vector of the uncontrolled structural system is written as

$$\mathbf{q}(t) = [q_{f1} \quad q_{e1} \quad q_{f2} \quad q_{e2} \quad q_{f3} \quad q_{e3} \quad q_{\mathrm{FA}} \quad q_{\mathrm{SS}} \quad q_m \quad \theta_m]^{\mathrm{T}} \tag{1}$$

where qfi and qei $(i = 1,2,3)$denote the first flapwise and edgewise modal coordinates of the three blades, respectively; q_{FA} and q_{SS} are the tower fore-aft and side-side generalized coordinates; $q_m$and θmdenote the effective translational and rotational coordinates of the monopile foundation .This generalized-coordinate definition is consistent with the 10-DOF idealization listed in Table 1.

Table 1. Generalized coordinates of the 10-DOF reduced-order model.

No.	Generalized coordinate	Description	Physical meaning
1	q_{f1}	First flapwise modal coordinate of Blade 1	Out-of-plane bending motion of Blade 1
2	q_{e1}	First edgewise modal coordinate of Blade 1	In-plane bending motion of Blade 1
3	q_{f2}	First flapwise modal coordinate of Blade 2	Out-of-plane bending motion of Blade 2
4	q_{e2}	First edgewise modal coordinate of Blade 2	In-plane bending motion of Blade 2
5	q_{f3}	First flapwise modal coordinate of Blade 3	Out-of-plane bending motion of Blade 3
6	q_{e3}	First edgewise modal coordinate of Blade 3	In-plane bending motion of Blade 3

 doi:10.20944/preprints202605.1085.v1

No.	Generalized coordinate	Description	Physical meaning
7	q_{FA}	Tower fore-aft bending coordinate	Dominant fore-aft vibration of the tower
8	q_{SS}	Tower side-side bending coordinate	Dominant side-side vibration of the tower
9	q_m	Effective translational coordinate of the monopile foundation	Horizontal translation of the monopile-foundation system
10	θ_m	Effective rotational coordinate of the monopile foundation	Rocking rotation of the monopile-foundation system

Using the Euler–Lagrange method, the governing equations of motion of the uncontrolled coupled system can be expressed as

$$\mathbf{M}\ddot{\mathbf{q}}(t) + \mathbf{C}\dot{\mathbf{q}}(t) + \mathbf{K}\mathbf{q}(t) = \mathbf{F}_w(t) + \mathbf{F}_{wa}(t) + \mathbf{F}_s(t) \quad (2)$$

where $\mathbf{M}$, $\mathbf{C}$, and $\mathbf{K}$ are the mass, damping, and stiffness matrices, respectively, and $\mathbf{F}_w(t)$,$\mathbf{F}_{wa}(t)$, and $\mathbf{F}_s(t)$ are the generalized load vectors corresponding to wind, wave, and seismic excitation. The mass matrix includes the contributions of the blades, rotor–nacelle assembly, tower, and monopile foundation, while the stiffness and damping matrices account for blade flexibility, tower bending stiffness, structural damping, and equivalent foundation effects. This form is consistent with dynamic models commonly used for response analysis of monopile-supported offshore wind turbines under environmental and seismic loading [6–10].

When a passive control device is installed inside the nacelle, the structural system is augmented by one additional degree of freedom associated with the absorber motion. The controlled system can then be written as

$$\mathbf{M}_c\ddot{\mathbf{q}}_c(t) + \mathbf{C}_c\dot{\mathbf{q}}_c(t) + \mathbf{K}_c\mathbf{q}_c(t) = \mathbf{F}_w(t) + \mathbf{F}_{wa}(t) + \mathbf{F}_s(t) + \mathbf{F}_c(t) \quad (3)$$

where $\mathbf{q}_c(t)$ is the augmented generalized displacement vector and $\mathbf{F}_c(t)$ is the interaction force induced by the attached controller. In the present study, the controller acts primarily in the tower fore-aft direction, which is the most critical direction for nacelle response in many passive control studies of offshore wind turbines. For the TMD, $\mathbf{F}_c(t)$ is generated by a linear spring–damper mechanism, whereas for the SSVI NES it arises from nonlinear restoring action together with unilateral impact interaction.

Several simplifying assumptions are adopted in the present model. First, only the dominant low-order structural motions are retained, because these modes govern the nacelle and tower responses that are most relevant to passive control. Second, the rotor–nacelle assembly is treated as a concentrated mass at the tower top. Third, blade and tower deformations are assumed to remain within the small-amplitude range required for modal superposition. Fourth, the monopile–soil interaction is represented by equivalent spring–damper elements rather than a full three-dimensional soil continuum model. Under these assumptions, the reduced-order formulation provides an efficient basis for comparing passive vibration-control strategies for monopile offshore wind turbines subjected to wind–wave–seismic loading. Therefore, the present model should be interpreted as a control-oriented comparative model rather than a high-fidelity aero-hydro-servo-soil interaction model.

2.2. Environmental Loading Modeling

The monopile offshore wind turbine is subjected to aerodynamic, hydrodynamic, and seismic excitation. To represent realistic operating and extreme conditions, wind and wave loading are introduced using established engineering models, while earthquake excitation is represented using recorded ground-motion data. The corresponding loading models are described in the following subsections.

 doi:10.20944/preprints202605.1085.v1

2.2.1. Wind Loading

The turbulent wind field is generated in accordance with IEC design requirements for offshore wind turbines using the Kaimal turbulence model and the TurbSim stochastic inflow simulator [27,28,31]. The stochastic fluctuation of wind speed is represented by the Kaimal spectrum, which is widely used in wind turbine simulations and is directly implemented in TurbSim for the generation of three-dimensional turbulent inflow fields.The wind speed at elevation z and time t is expressed as

$$U(z,t) = \bar{U}(z) + u'(z,t) \tag{4}$$

where $\bar{U}(z)$ is the mean wind speed profile and $u'(z,t)$ is the fluctuating turbulence component.

The Kaimal spectrum for the longitudinal turbulence component is given by

$$S_u(f) = \frac{4\sigma_u^2 L_u/\bar{U}_h}{(1+6fL_u/\bar{U}_h)^{5/3}} \tag{5}$$

where f is the frequency, σ_u is the standard deviation of the longitudinal wind-speed fluctuation, L_u is the longitudinal turbulence scale, and $\bar{U}_h$ is the mean wind speed at hub height [24]. Based on this spectral model, turbulent wind time histories are generated for the dynamic simulations. A representative turbulent wind speed time history is shown in Figure 2.

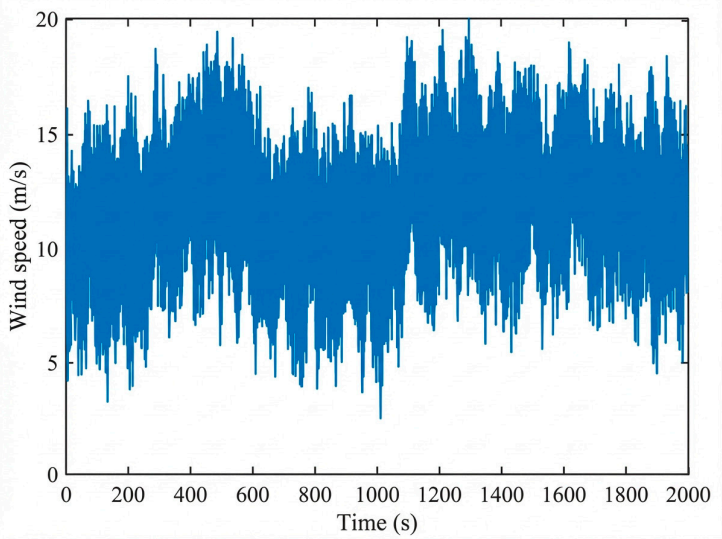

Figure 2. Turbulent wind speed time history generated using the Kaimal spectrum.

Using the generated three-dimensional turbulent wind field, the aerodynamic loads acting on the rotating blades are evaluated using blade element momentum theory. The aerodynamic model follows the standard BEM-based framework implemented in AeroDyn-type wind turbine analysis, in which blade element aerodynamics are coupled with momentum theory for efficient prediction of rotor loads [33,34]. To improve the aerodynamic prediction under practical operating conditions, the model incorporates the Prandtl tip-loss correction and the high-induction correction commonly associated with the Glauert/Buhl formulation [33,35]. The resulting blade forces are transformed into generalized forces and introduced into the structural equations of motion.

In the reduced-order model adopted here, only the dominant aerodynamic excitation transmitted from the rotor to the tower–nacelle system is retained. Higher-order aeroelastic effects that are not directly related to the global vibration-control problem are not explicitly considered. This treatment is consistent with the control-oriented purpose of the present model.

 doi:10.20944/preprints202605.1085.v1

2.2.2. Wave Loading

The wave-induced hydrodynamic force acting on the monopile foundation is calculated using the Morison equation, which is commonly adopted for slender offshore members whose diameters are small relative to the incident wavelength [29]. The horizontal wave force per unit length can be written as

$$\mathrm{d}F_{wa}(z,t) = \frac{1}{2}\rho_w C_D D|u_w(z,t)|u_w(z,t)\,\mathrm{d}z + \rho_w C_M \frac{\pi D^2}{4}\dot{u}_w(z,t)\,\mathrm{d}z \tag{6}$$

where ρ_w is the seawater density, D is the monopile diameter,C_D and C_M are the drag and inertia coefficients, respectively, and $u_w(z,t)$ and $\dot{u}_w(z,t)$ are the horizontal water-particle velocity and acceleration as well as the corresponding structural motion.

The irregular sea state is described using the JONSWAP spectrum, which is widely used for fetch-limited wind-generated waves in offshore engineering applications [30]. The corresponding spectral density function is expressed as

$$S_\eta(f) = \alpha g^2(2\pi)^{-4} f^{-5} \exp\left[-\frac{5}{4}\left(\frac{f_p}{f}\right)^4\right]\gamma^{\exp\left[-\frac{(f-f_p)^2}{2\sigma^2 f_p^2}\right]} \tag{7}$$

where f_p is the peak frequency, γ is the peak enhancement factor, alpha is the Phillips constant, g is the gravitational acceleration, and σ is the spectral width parameter [30]. The adopted JONSWAP spectrum is shown in Figure 3. This spectrum defines the frequency distribution of wave energy and provides the basis for generating the irregular wave-elevation time histories used in the hydrodynamic loading analysis.

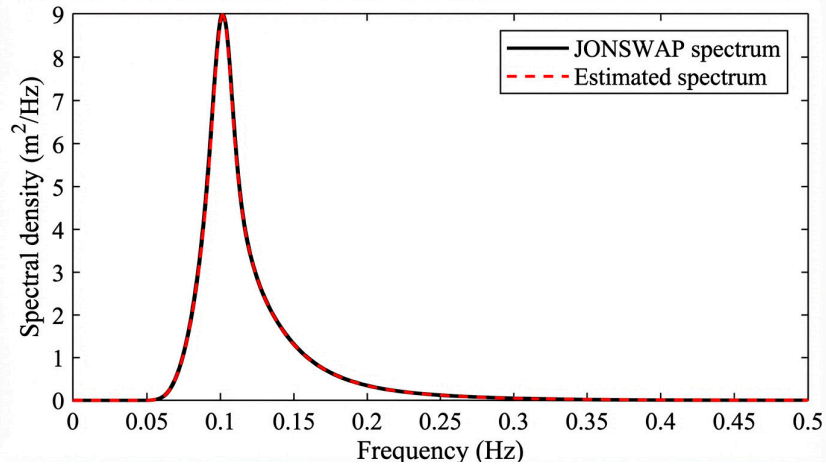

Figure 3. JONSWAP spectrum adopted for irregular sea-state modeling.

Using the JONSWAP spectrum, irregular wave-elevation time histories are generated in the time domain. A representative wave-elevation time history is shown in Figure 4, which reflects the non-periodic characteristics of the irregular sea state considered in this study. The corresponding water-particle kinematics are determined based on linear wave theory and substituted into the Morison equation to calculate the distributed hydrodynamic load on the submerged portion of the monopile. The generalized wave-force vector is then obtained by projecting the distributed hydrodynamic load onto the retained structural modes. This treatment provides an efficient and physically consistent representation of wave loading for repeated time-domain simulations of the reduced-order offshore wind turbine model.

 doi:10.20944/preprints202605.1085.v1

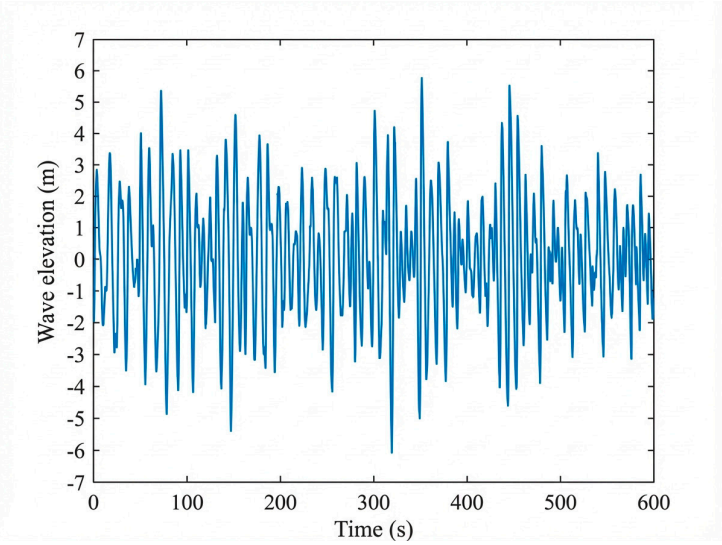

Figure 4. Representative irregular wave-elevation time history generated from the JONSWAP spectrum.

2.2.3. Seismic Loading

Although offshore wind turbines are commonly analyzed under wind and wave excitation, seismic action may become important for turbines located in coastal and seismically active regions [8–15]. In the present study, earthquake excitation is introduced as horizontal base acceleration applied at the monopile foundation. Under base excitation, the structural dynamic equation can be written as

$$\mathbf{M}\ddot{\mathbf{q}}(t) + \mathbf{C}\dot{\mathbf{q}}(t) + \mathbf{K}\mathbf{q}(t) = \mathbf{F}_w(t) + \mathbf{F}_{wa}(t) - \mathbf{M}\Gamma a_g(t) \quad (8)$$

where $a_g(t)$ is the ground-acceleration time history and Γ is the influence vector associated with the base motion.

To represent realistic seismic input, fifteen recorded ground motions are selected from the PEER NGA-West2 database [32]. The selected records cover a range of earthquake magnitudes, site conditions, source-to-site distances, peak ground accelerations, spectral accelerations, and Arias intensities. This selection allows the seismic sensitivity of the monopile offshore wind turbine to be examined under diverse ground-motion characteristics. The selected records are summarized in Table 2.

Table 2. Selected ground motion records from the PEER NGA-West2 database.

No.	Earthquake	RSN	Vs30 (m/s)	Mw	Sa (g), x/y	PGA (m/s²), x/y	AI (m/s)	Rjb (km)
1	Chi-Chi_ Taiwan	1535	535.23	7.62	0.251 / 0.341	1.442 / 1.592	1.6	13.04
2	Kern County	15	385.63	7.36	0.038 / 0.040	1.422 / 1.501	0.6	38.42
3	El Mayor-Cucapah_	5975	231.83	7.20	0.135 / 0.113	1.714 / 2.665	2.4	19.12
4	Chi-Chi_ Taiwan	1506	401.96	7.62	0.175 / 0.244	2.491 / 1.575	2.3	19.00
5	Imperial Valley-06	164	471.03	6.53	0.034 / 0.067	1.571 / 1.448	1.3	15.19
6	Manjil_ Iran	1633	723.05	7.37	0.087 / 0.163	5.048 / 4.529	7.5	12.55

 doi:10.20944/preprints202605.1085.v1

No.	Earthquake	RSN	Vs30 (m/s)	Mw	Sa (g), x/y	PGA (m/s²), x/y	AI (m/s)	Rjb (km)
7	Imperial Valley-02	6	213.34	6.95	0.074 / 0.089	2.493 / 1.474	1.6	6.09
8	Chi-Chi_ Taiwan	1247	175.88	7.62	0.082 / 0.125	0.778 / 1.009	0.4	50.61
9	Darfield_ New Zealand	6888	198.90	7.00	0.261 / 0.136	1.808 / 1.645	1.3	19.89
10	San Fernando	88	389.10	6.61	0.060 / 0.021	1.519 / 1.519	0.2	24.69
11	Kobe_ Japan	1120	256.40	6.90	0.210 / 0.276	6.060 / 6.583	8.7	1.46
12	Iwate_ Japan	5818	512.96	6.90	0.185 / 0.069	3.882 / 6.893	7.3	12.83
13	Duzce_ Turkey	1605	281.36	7.14	0.238 / 0.249	2.784 / 5.052	2.9	0.00
14	Taiwan SMART1	582	357.03	7.30	0.078 / 0.154	1.213 / 1.613	0.8	54.80
15	Chuetsu-oki_ Japan	4850	561.19	6.80	0.231 / 0.226	6.293 / 5.683	1.7	13.68

By using multiple recorded ground motions rather than a single representative accelerogram, the variability of structural response under seismic excitation can be evaluated more consistently. This treatment is particularly important for monopile offshore wind turbines, whose flexible low-frequency dynamics may lead to record-dependent response amplification under earthquake loading [8–15,32].

For clarity, the loading scenarios considered in the present study are summarized in Table 3. These load cases are designed to evaluate baseline serviceability response, seismic sensitivity, multi-hazard response, and robustness under structural-frequency detuning.

Table 3. Load cases considered in the present study.

Load case	Wind	Wave	Seismic	Purpose
LC1	✓	✓	–	Baseline serviceability response and nominal controller comparison
LC2	–	–	✓	Seismic sensitivity and transient response assessment
LC3	✓	✓	✓	Multi-hazard resilience assessment under coupled environmental and seismic actions
LC4	✓	✓	–	Robustness assessment under structural-frequency detuning

Compared with a single-hazard framework, these loading scenarios provide a more comprehensive basis for evaluating passive vibration-control performance. In particular, LC3 is used to examine the structural response under combined environmental and seismic actions, while LC4 is used to assess whether the controller can retain its effectiveness when the structural frequency deviates from the nominal design value.

2.3. Performance Metrics

To evaluate the effectiveness and robustness of the proposed single-sided vibro-impact nonlinear energy sink, several response- and device-oriented performance metrics are adopted. The RMS nacelle fore-aft displacement is used as the primary indicator under stochastic wind–wave excitation, whereas peak response quantities are used to characterize extreme structural demand, particularly under transient seismic excitation. In addition, absorber stroke demand and accumulated

 doi:10.20944/preprints202605.1085.v1

dissipated energy are considered to assess installation feasibility and energy-dissipation behavior. For detuned conditions, a robustness index is introduced to quantify the retained control effectiveness. These metrics provide a consistent basis for comparing the SSVI NES with the benchmark TMD and for assessing passive vibration-control performance under nominal and off-design conditions [4–8,16–22].

For a generic structural response quantity $x(t)$, the root-mean-square (RMS) value over a simulation duration T is defined as

$$x_{\mathrm{RMS}} = \sqrt{\frac{1}{T}\int_0^T x^2(t)\,\mathrm{d}t} \tag{9}$$

The RMS metric reflects the sustained vibration level of the system and is therefore adopted as the primary response index in the present study. The corresponding peak response is defined as

$$x_{\mathrm{peak}} = \max_{0\le t\le T} |x(t)| \tag{10}$$

which is used to characterize the maximum instantaneous structural demand, particularly under transient seismic excitation.

To quantify the control effectiveness relative to the uncontrolled structure, the response reduction ratio is defined as

$$\eta_x = \frac{x_{\mathrm{un}} - x_{\mathrm{ctrl}}}{x_{\mathrm{un}}} \tag{11}$$

where x_{un} and x_{ctrl} denote the selected response metric of the uncontrolled and controlled systems, respectively. In the present study, x may represent either the RMS or peak value of nacelle displacement or acceleration. A larger value of η_x indicates better vibration mitigation performance.

Because nacelle space is limited, the absorber stroke demand is also taken as an important engineering metric. It is defined as

$$y_{max} = \max_{0\le t\le T} |y(t)| \tag{12}$$

where$y(t)$ is the relative displacement of the absorber mass with respect to the nacelle. For the TMD, this quantity corresponds to the required working stroke of the linear absorber. For the SSVI NES, it denotes the effective motion range of the impact oscillator. This metric is particularly important for nacelle-integrated passive control because excessive stroke demand may conflict with practical installation constraints.

As a supplementary indicator for interpreting the vibration-mitigation mechanism, the accumulated dissipated energy of the control device is also evaluated as

$$E_{\mathrm{d}} = \int_0^T P_{\mathrm{d}}(t)\,\mathrm{d}t \tag{13}$$

where $P_d(t)$ is the instantaneous dissipated power. For the TMD, the dissipated power is written as

$$P_{\mathrm{d,TMD}}(t) = c_t\,\dot{y}^2(t) \tag{14}$$

where c_t is the TMD damping coefficient. For the SSVI NES, the dissipated energy includes both viscous dissipation and impact-induced energy loss. Therefore, this metric is used to interpret the nonlinear energy-transfer and impact-assisted dissipation mechanisms of the SSVI NES [22–26].

To assess off-design performance, frequency-detuning scenarios are considered and the retained control effectiveness is measured using the robustness index

$$R_x = \frac{\eta_x(\delta)}{\eta_x(0)} \times 100\% \tag{15}$$

where $\eta_x(0)$ denotes the response at the resonant condition, and $\eta_{\mathrm{x}}(\delta)$ denotes the response under frequency detuning δ.The robustness metric is expressed as a percentage to ensure consistency with

 doi:10.20944/preprints202605.1085.v1

the detuning analysis presented in Section 4.4. A larger value indicates that the controller retains its vibration-mitigation capability more effectively under off-design structural-frequency variations.

For seismic loading cases involving multiple ground motions, the corresponding response metrics are summarized using the ensemble mean

$$\bar{x} = \frac{1}{N_g}\sum_{i=1}^{N_g} x_i \tag{16}$$

where N_g is the number of ground-motion records and x_i is the corresponding response metric for the i-th record [32].

In the following sections, the RMS nacelle fore-aft displacement is taken as the primary performance metric, while peak response, absorber stroke demand, dissipated energy, and robustness index are used as complementary indicators. Together, these metrics allow the proposed SSVI NES to be evaluated not only in terms of nominal response reduction, but also in terms of practical motion demand and robustness under uncertain structural-frequency conditions.

3. Dynamic Characteristics and Baseline Response of the Uncontrolled System

This section investigates the dynamic characteristics and baseline response of the uncontrolled monopile offshore wind turbine. Since monopile offshore wind turbines are flexible low-frequency systems whose responses are strongly affected by coupled blade–tower–foundation dynamics, it is necessary to first examine the modal characteristics of the reduced-order model [1,4,7,8,10–15]. The uncontrolled responses under representative wind–wave and seismic loading conditions are then analyzed to establish the reference response level for controller comparison. Finally, the relationship between seismic intensity measures and structural response is discussed using the selected PEER ground-motion records [32].

3.1. Modal Characteristics of the Reduced-Order Model

The modal characteristics of the reduced-order model are first examined with reference to benchmark results reported for the NREL 5 MW offshore wind turbine [1]. For passive vibration-control analysis, the most important modes are the low-order global tower and blade–tower–foundation modes, because these modes dominate the nacelle displacement, tower-top acceleration, and controller–structure interaction [4,7,8,14,15].

The benchmark natural frequencies reported for the NREL 5 MW offshore wind turbine using FAST, ADAMS, and a no-soil model are summarized in Table 4 [1,36]. As shown in the table, the first two natural frequencies are concentrated around 0.32–0.34 Hz, indicating the low-frequency and flexible nature of the monopile-supported offshore wind turbine. These low-order modes are particularly important for nacelle-mounted passive control devices, because the controller is mainly designed to suppress the dominant fore-aft vibration of the tower–nacelle system [4,7,8].

Table 4. Benchmark natural frequencies of the NREL 5 MW offshore wind turbine reported in previous studies.

Mode	FAST (Hz)	ADAMS (Hz)	No-soil model (Hz)
1	0.3220	0.3264	0.3420
2	0.3340	0.3295	0.3429
3	0.6605	0.6194	0.7499
4	0.6764	0.6396	0.7556
5	0.6775	0.6786	0.7712
6	0.6999	0.7119	1.1077
7	1.0893	1.0840	1.1089

 doi:10.20944/preprints202605.1085.v1

The comparison in Table 4 shows that the low-order modal frequencies obtained from different modeling approaches are relatively close, whereas higher-order modes exhibit larger variation. This is reasonable because higher-order blade and tower modes are more sensitive to detailed modeling assumptions, including blade flexibility, aerodynamic coupling, foundation representation, and soil–structure interaction [1,10,11,36]. In contrast, the dominant low-frequency global modes are more stable and are therefore suitable as the main basis for control-oriented modeling.

Accordingly, the present reduced-order model is considered appropriate for comparative vibration-control analysis. Its purpose is not to reproduce every high-order aero-hydro-servo-elastic feature of the offshore wind turbine, but to preserve the dominant structural dynamics that govern nacelle response and passive controller performance [4–8]. This modeling strategy provides an efficient basis for repeated time-domain simulations, parametric studies, and frequency-detuning analysis.

3.2. Baseline Dynamic Response without Control

After examining the modal characteristics, the baseline dynamic response of the uncontrolled monopile offshore wind turbine is evaluated under the representative loading cases defined in Table 3. This step establishes the reference response level before installing any passive control device. The nacelle fore-aft response is selected as the primary response quantity because it directly reflects the global vibration of the tower–nacelle system and is closely related to the working direction of the nacelle-mounted controller [4,7,8].

Under combined wind–wave loading, the uncontrolled system exhibits sustained low-frequency vibration, which is mainly governed by the global bending response of the flexible tower–foundation system [4–8]. Because both turbulent wind and irregular waves are stochastic excitations, the nacelle and tower-top responses fluctuate continuously with time. A representative uncontrolled response history is shown in Figure 5.

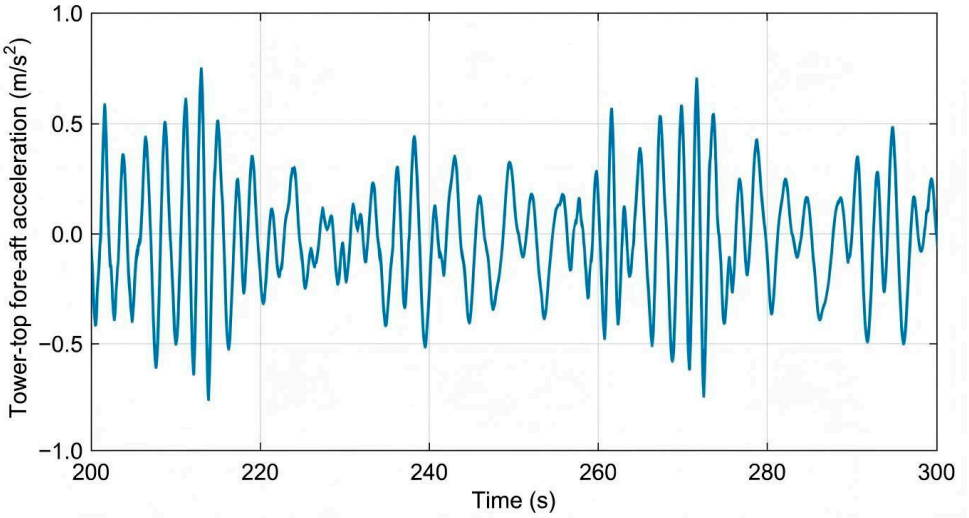

Figure 5. Uncontrolled tower-top acceleration response under combined wind-wave loading.

The response shown in Figure 5 indicates that wind–wave loading produces continuous dynamic excitation rather than a short-duration impulse. This type of sustained vibration may contribute to fatigue accumulation and serviceability concerns during long-term operation [4–8]. Therefore, reducing the RMS response under wind–wave loading is important for evaluating the effectiveness of passive vibration-control devices.

When seismic excitation is introduced, the response characteristics become different from those under wind–wave loading. Earthquake excitation produces transient response amplification, and the response level varies significantly among different ground-motion records [8–15,32]. Representative

 doi:10.20944/preprints202605.1085.v1

nacelle fore-aft displacement and acceleration responses under selected seismic records are shown in Figure 6.

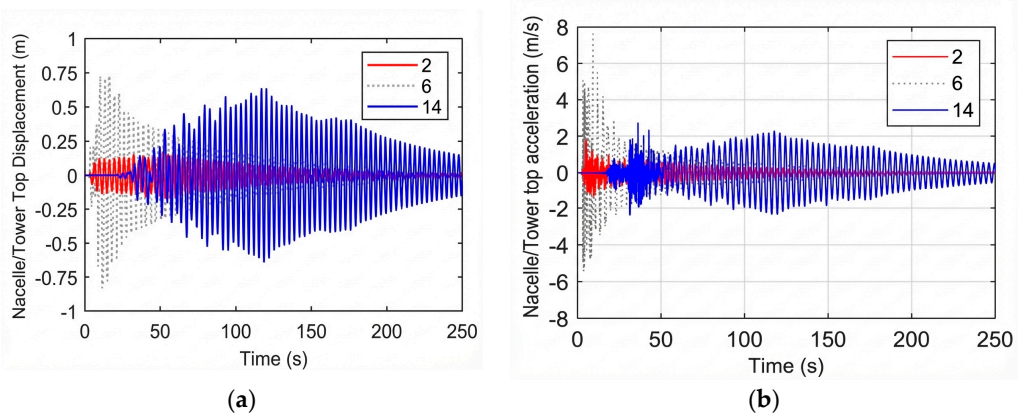

(a) (b)

Figure 6. Representative responses of the uncontrolled offshore wind turbine under selected earthquake records: (a) nacelle fore-aft displacement; (b) nacelle fore-aft acceleration.

As shown in Figure 6, some earthquake records generate much larger structural responses than others. This record-to-record variability indicates that the seismic response of the monopile offshore wind turbine is not governed only by peak ground acceleration, but also by the frequency content and duration of the input motion [8–15,32]. Because the turbine is a low-frequency flexible structure, seismic components close to the dominant structural frequency may lead to significant response amplification.

Overall, the baseline response analysis shows that wind–wave loading mainly causes sustained vibration, whereas seismic loading may induce strong transient amplification. These uncontrolled responses provide the reference basis for the subsequent comparison between the optimized TMD and the proposed SSVI NES.

3.3. Seismic Intensity–Response Relationship

To further clarify the seismic sensitivity of the uncontrolled system, the relationship between seismic intensity measures and structural response is examined using the selected PEER ground-motion records [32]. The maximum nacelle fore-aft displacement is adopted as the representative response quantity. Spectral acceleration and peak ground acceleration are selected as the seismic intensity measures for comparison because they are commonly used to characterize earthquake excitation amplitude and frequency-dependent seismic demand.

The maximum response is defined as

$$x_{\max} = \max_{0 \le t \le T} |x(t)| \tag{17}$$

where $x(t)$ denotes the nacelle fore-aft displacement time history. For each selected ground-motion record, the maximum nacelle response is calculated and compared with the corresponding seismic intensity measures. The results are shown in Figure 7.

 doi:10.20944/preprints202605.1085.v1

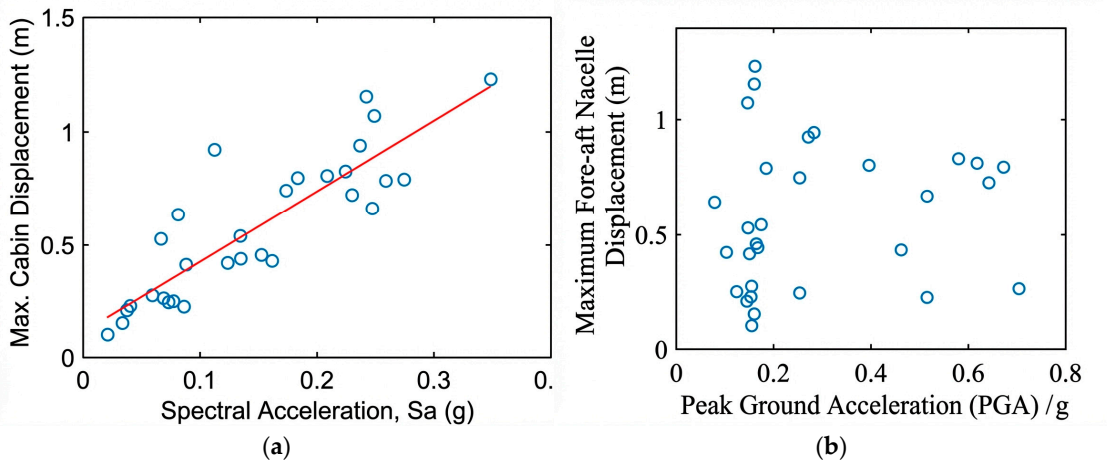

Figure 7. Maximum nacelle fore-aft displacement versus seismic intensity measures: (a) versus spectral acceleration S_a; (b) versus peak ground acceleration PGA.

As shown in Figure 7a, the maximum nacelle displacement exhibits a clearer increasing trend with spectral acceleration. In contrast, the relationship between maximum nacelle displacement and PGA in Figure 7b is more scattered. This indicates that spectral acceleration is a more suitable intensity measure for characterizing the seismic demand of the monopile offshore wind turbine, because it reflects the frequency-dependent characteristics of earthquake excitation more directly than PGA [8–15,32].

This result is consistent with the dynamic characteristics discussed in Section 3.1. Since the structural response is dominated by low-frequency global modes, an intensity measure that accounts for frequency-dependent excitation characteristics can better represent the seismic demand than PGA alone [8–15]. Therefore, the seismic response of monopile offshore wind turbines should be interpreted not only in terms of excitation amplitude, but also in terms of the compatibility between ground-motion frequency content and the dominant structural modes.

The results in this section demonstrate that the uncontrolled monopile offshore wind turbine is sensitive to both sustained environmental loading and transient seismic excitation, which is consistent with previous studies on offshore wind turbine dynamic response under wind–wave and seismic loading [4–15]. The baseline response characteristics identified here provide the necessary reference for evaluating the nominal control performance and detuning robustness of the proposed SSVI NES in Section 4.

4. Vibration-Control Performance and Robustness Assessment

In this section, the vibration-control performance of the proposed single-sided vibro-impact nonlinear energy sink (SSVI NES) is evaluated through comparison with a conventional tuned mass damper (TMD). Following the baseline response analysis in Section 3, the comparison is conducted under the load cases defined in Table 3. The purpose of this section is not only to compare response-reduction efficiency, but also to assess the practical suitability of the two passive control devices for nacelle-integrated implementation in monopile offshore wind turbines. Therefore, attention is given to three aspects that are important for structural safety and serviceability: nominal vibration mitigation, absorber motion demand, and robustness under structural-frequency detuning [2,4–8,14,15,22].

4.1. Optimized TMD as a Benchmark Passive Controller

The tuned mass damper is adopted as the benchmark passive control device because it is one of the most widely used vibration absorbers for offshore wind turbine applications [4–8,14,15,22]. In the present study, the TMD is installed inside the nacelle and arranged in the tower fore-aft direction,

 doi:10.20944/preprints202605.1085.v1

which corresponds to the dominant response direction considered in the baseline analysis. To ensure a fair comparison, the TMD parameters are optimized before being compared with the proposed SSVI NES. This means that the SSVI NES is evaluated against a strong linear passive-control baseline rather than an arbitrarily selected TMD configuration [4,7,8,14,15,22].

For a prescribed mass ratio, the optimal TMD parameters are obtained by minimizing the RMS nacelle fore-aft displacement under the nominal design condition. The optimization problem is expressed in Equations (18) and (19).

$$\min_{f_r,\xi_t} J\,(f_r,\xi_t) = x_{\mathrm{RMS}} \tag{18}$$

where

$$f_r = \frac{\omega_t}{\omega_1},\quad \xi_t = \frac{c_t}{2m_t\omega_t},\quad \mu = \frac{m_t}{M_{\mathrm{eff}}} \tag{19}$$

in which f_r is the TMD frequency ratio, ξ_t is the TMD damping ratio, and μ is the absorber mass ratio. Here,ω_t and ω_1 denote the natural frequencies of the TMD and the dominant structural mode, respectively,while $m_t, c_t,$ and M_{eff} represent the TMD mass, damping coefficient, and effective modal mass of the controlled structure. For each candidate parameter pair (f_r, ξ_t),time-domain simulations are carried out and the corresponding RMS nacelle fore-aft displacement is evaluated. The corresponding optimization contour is shown in Figure 8.

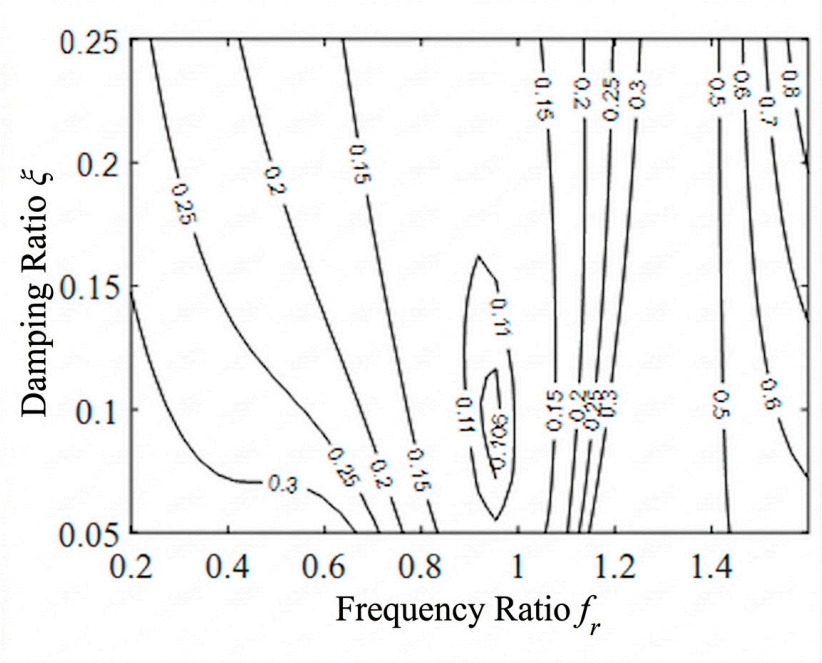

Figure 8. Optimization contour of the TMD in the frequency-ratio–damping-ratio parameter space.

As shown in Figure 8, the vibration-control performance of the TMD is highly dependent on the frequency ratio and damping ratio. A favorable control effect is obtained only within a relatively narrow region around the optimal tuning condition. This confirms the typical narrow-band characteristic of a linear tuned absorber, which has also been reported in previous TMD-based offshore wind turbine studies [4,7,8,14,15,22]. From an engineering perspective, this feature is important because the dynamic characteristics of offshore wind turbines may vary during long-term service due to foundation flexibility, soil–structure interaction, scour, operating-state changes, and modeling uncertainty [2,3,10,11].

The optimal TMD tuning parameters for different mass ratios are summarized in Table 5.

 doi:10.20944/preprints202605.1085.v1

Table 5. Optimal TMD tuning parameters identified by numerical search for representative mass ratios.

Mass ratio,μ	Optimal frequency ratio, f_r	Optimal damping ratio, ξ_t
0.01	0.985	0.060
0.02	0.975	0.085
0.03	0.965	0.100
0.04	0.955	0.112
0.05	0.939	0.126
0.06	0.929	0.141
0.07	0.918	0.153
0.08	0.907	0.160
0.09	0.898	0.170
0.10	0.888	0.182

Table 5 shows that the optimal frequency ratio decreases as the mass ratio increases, whereas the optimal damping ratio increases. This trend indicates that the TMD design is closely associated with the selected absorber mass and the target structural frequency. Although increasing the absorber mass can improve vibration suppression, it may also lead to practical challenges related to nacelle installation, device weight, and available internal space [4,7,8,22].

The time-history responses of the offshore wind turbine controlled by the optimized TMD are shown in Figure 9.

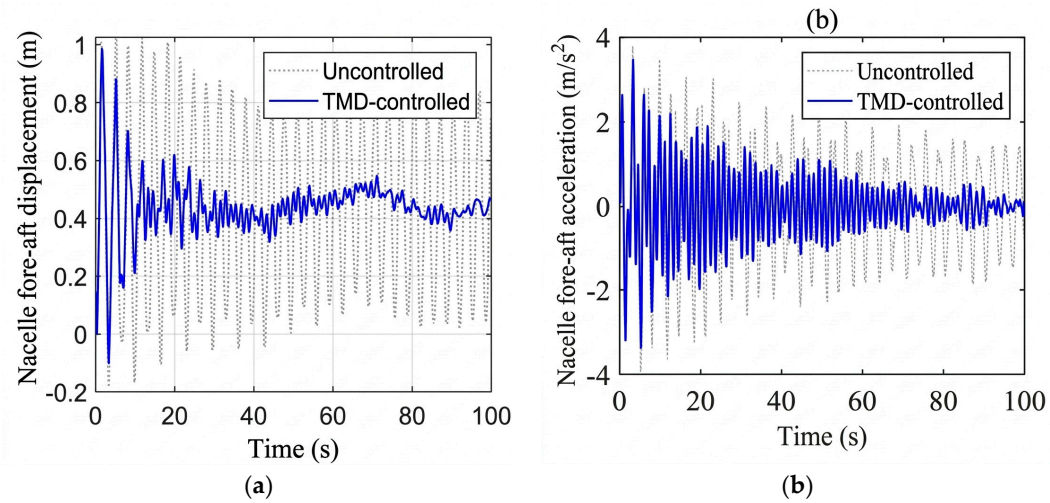

Figure 9. Time-history responses of the offshore wind turbine with the optimized TMD under the design condition: (a) nacelle fore-aft displacement; (b) nacelle fore-aft acceleration.

Figure 9 shows that the optimized TMD effectively reduces both nacelle displacement and acceleration under the design condition. Therefore, the optimized TMD provides a meaningful benchmark for assessing the proposed SSVI NES. However, because its performance depends on accurate tuning, the TMD may become less reliable when the actual structural frequency deviates from the nominal design value [4,7,8,14,15,22]. This limitation motivates the subsequent comparison with the SSVI NES from the perspectives of motion demand and detuning robustness.

4.2. Parameter Influence of the SSVI NES

Unlike the TMD, the SSVI NES does not rely on a single sharply tuned linear resonance condition. Its control performance is governed by nonlinear energy transfer, unilateral impact interaction, and

 doi:10.20944/preprints202605.1085.v1

impact-induced energy dissipation [16–21]. Therefore, the main design parameters of the SSVI NES are examined to identify a practical parameter range suitable for nacelle-mounted application.

The dimensionless parameters of the SSVI NES are defined in Equation (20), and the RMS nacelle fore-aft displacement used for evaluating control effectiveness is defined in Equation (21).

$$f_r = \frac{\omega_n}{\omega_1}, B_r = \frac{k_c}{k_{\text{ref}}}, G_r = \frac{g_0}{x_{\text{ref}}} \tag{20}$$

where f_r is the effective frequency ratio of the SSVI NES, B_r is the contact stiffness ratio, and G_r is the gap ratio. Here, ω_n and ω_1 denote the nominal frequency of the SSVI NES and the dominant structural frequency of the primary system, respectively, while k_c and g_0 represent the contact stiffness and the impact gap. The control performance is evaluated using the RMS nacelle fore-aft displacement,

$$J(f_r, B_r, G_r) = x_{\text{RMS}} \tag{21}$$

where smaller values of J indicate better vibration mitigation performance.

The first key parameter examined is the gap ratio G_r. The gap determines when the absorber contacts the single-sided barrier and therefore controls the activation of the impact mechanism [18–21]. If the gap is too small, impacts may occur too frequently and restrict the development of effective relative motion. If the gap is too large, the impact mechanism may not be sufficiently activated under moderate structural vibration. Therefore, an appropriate intermediate gap is necessary to balance vibration reduction and absorber motion demand. The influence of the gap ratio is shown in Figure 10.

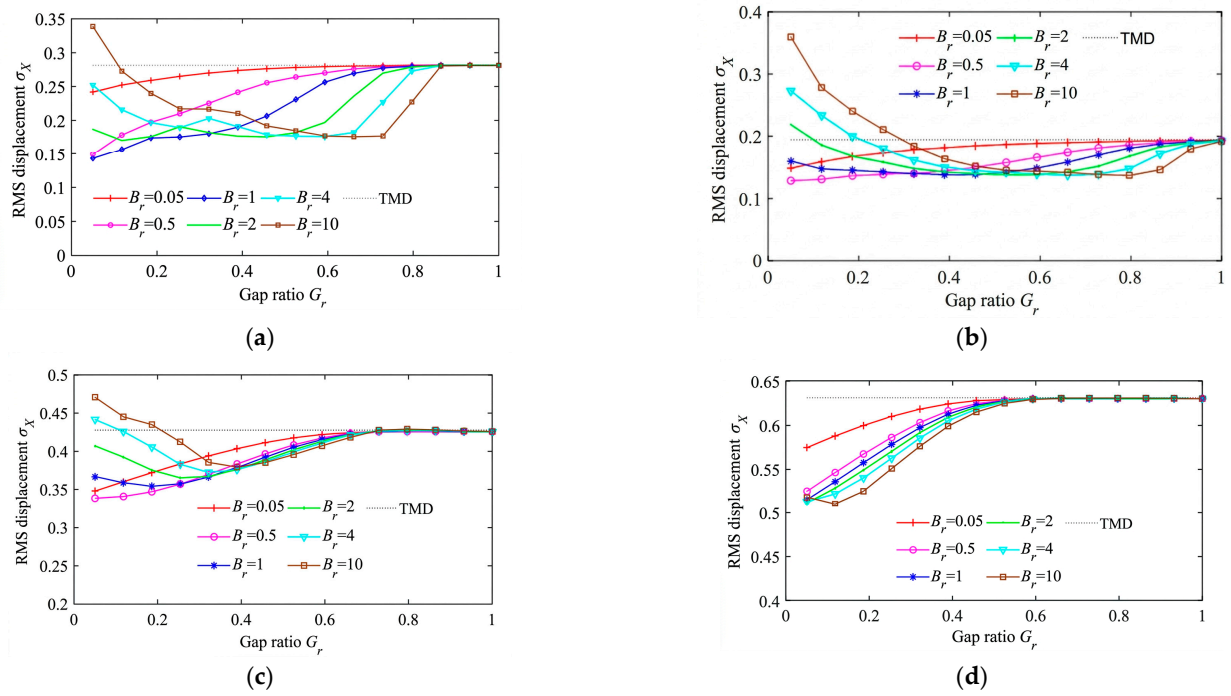

Figure 10. Parametric effect of gap ratio on the RMS nacelle fore-aft displacement of the SSVI NES under different frequency ratios: (a) f_r = 0.4; (b) f_r = 0.7; (c) f_r = 1.3; (d) f_r = 1.6.

Figures 10a–d indicate that the control performance of the SSVI NES is sensitive to the gap ratio under different frequency ratios. Nevertheless, the effective region is not limited to a single isolated optimum; instead, a practical interval can be identified in which satisfactory vibration mitigation is maintained together with acceptable absorber motion. This result suggests that the impact gap acts not merely as a geometric parameter, but also as a regulator of the onset and intensity of impact-assisted energy dissipation.

 doi:10.20944/preprints202605.1085.v1

The second parameter is the contact stiffness ratio B_r, which governs the intensity of the impact event between the oscillator and the single-sided barrier. When the contact stiffness is too low, the impact-induced dissipation is insufficient and the additional nonlinear mechanism cannot be fully activated. As the contact stiffness increases, the structural response is progressively reduced because the collision process becomes more effective in extracting and dissipating vibration energy. However, once the stiffness exceeds a certain level, the improvement becomes much less pronounced. This saturation trend indicates that excessively large contact stiffness is not necessary from an engineering implementation perspective.

Figure 11a–d indicate that increasing the contact stiffness ratio improves the vibration-mitigation performance of the SSVI NES at low stiffness levels, whereas the benefit gradually diminishes at higher stiffness levels. This suggests that, although a sufficiently stiff contact interface is required to ensure effective impact-assisted dissipation, excessively large stiffness provides limited additional benefit. Therefore, a moderate-to-high contact stiffness is generally preferable from an engineering viewpoint .

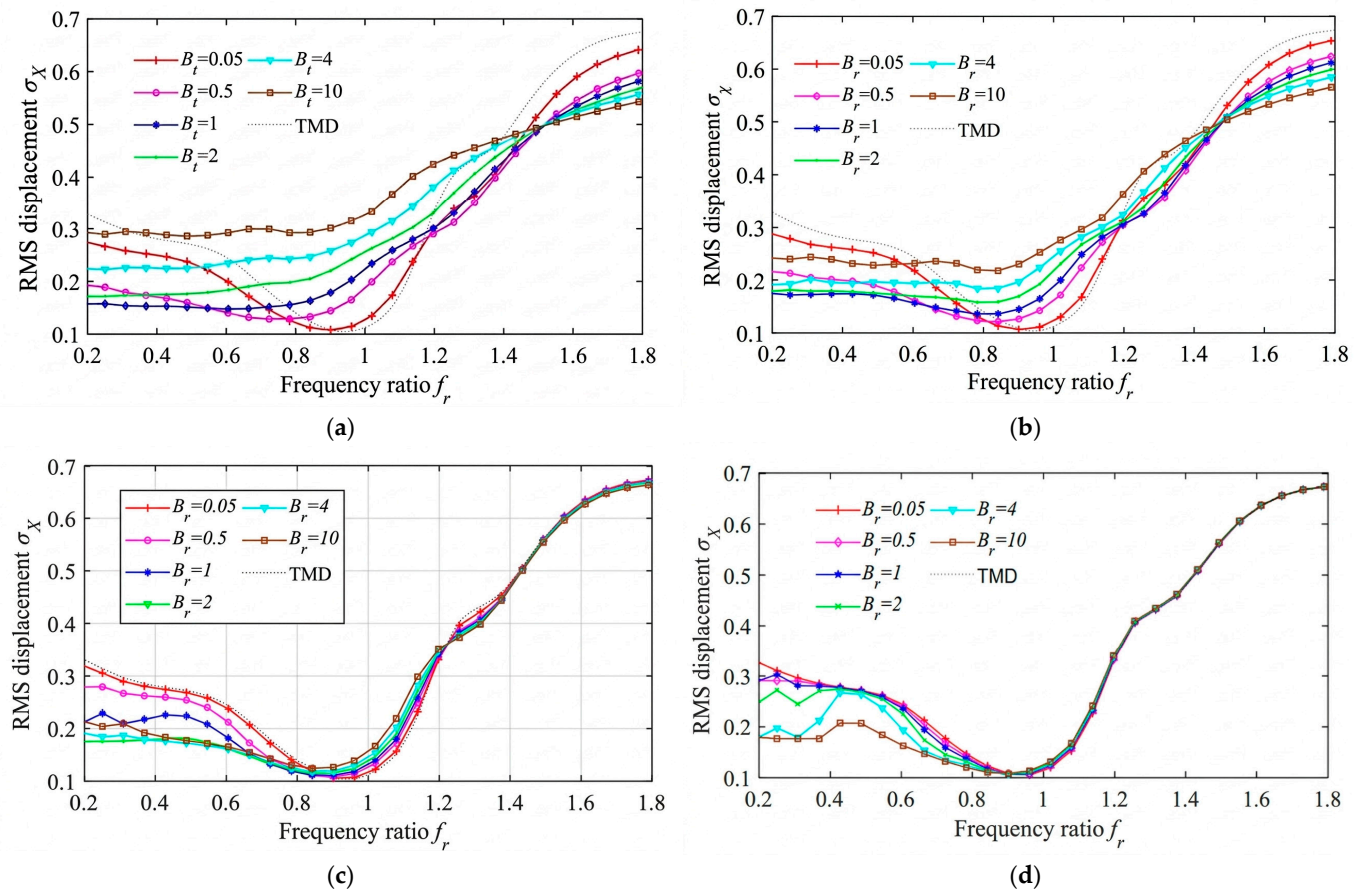

Figure 11. Parametric effect of contact stiffness ratio on the RMS nacelle fore-aft displacement of the SSVI NES under different gap ratios: (a) G_r = 0.1; (b) G_r = 0.2; (c) G_r = 0.5; (d) G_r = 0.75.

To further evaluate the engineering applicability of the SSVI NES, the combined influence of the gap ratio and contact stiffness ratio on both structural response and absorber motion is examined. In the following analysis, the tuning frequency ratio is fixed at $f_r = 0.9$, and the effects of different gap ratios and contact stiffness ratios on the RMS nacelle fore-aft displacement and the maximum absorber displacement are assessed simultaneously.

Figure 12a,b present the effects of the gap ratio and contact stiffness ratio on the vibration mitigation performance and motion demand of the SSVI NES at $f_r = 0.9$. It can be seen from Figure 12a that, when the contact stiffness ratio becomes sufficiently large, its influence on the RMS nacelle

 doi:10.20944/preprints202605.1085.v1

fore-aft displacement gradually diminishes. Moreover, for relatively large gap ratios, the control effectiveness of the SSVI NES becomes comparable to that of the TMD. Meanwhile, Figure 12b indicates that a larger contact stiffness ratio provides a stronger limitation on the maximum absorber displacement. Therefore, the results confirm that, for nacelle installation under limited available space, a suitable combination of gap ratio and contact stiffness ratio is essential for fully exploiting the performance potential of the SSVI NES.

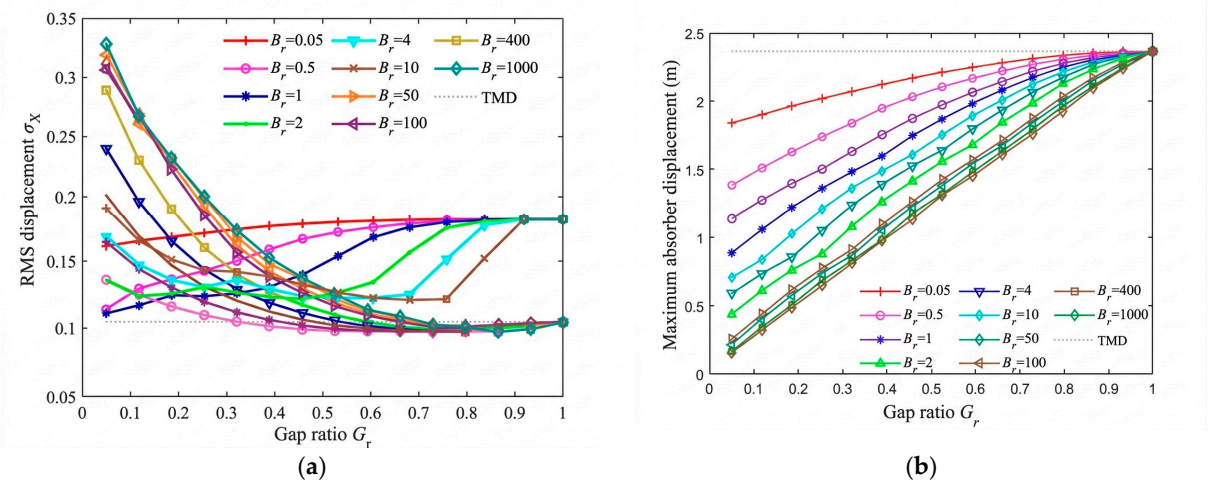

(a) (b)

Figure 12. Influence of gap ratio and contact stiffness ratio on the performance and stroke demand of the SSVI NES at $f_r = 0.9$: (a) RMS nacelle fore-aft displacement; (b) Maximum absorber displacement.

Based on the parametric results shown in Figures 10–12, Table 6 summarizes the parameter ranges associated with satisfactory vibration mitigation and acceptable absorber motion.

Table 6. Recommended parameter ranges of the SSVI NES identified from the parametric study.

Parameter	Recommended range	Influence on performance	Design implication
Frequency ratio, f_r	0.8–1.0	Governs nonlinear interaction bandwidth; effective mitigation is maintained over a relatively broad interval	Select near but slightly below unity to improve tolerance to frequency variation
Contact stiffness ratio, B_r	10–100	Controls impact intensity and energy dissipation; performance improves initially and then tends to saturate	Use moderate-to-high stiffness; excessively large values provide limited additional benefit
Gap ratio, G_r	0.4–0.8	Determines activation of the impact mechanism and the balance between free motion and impacts	Choose an intermediate gap to achieve effective dissipation while limiting stroke demand

The representative SSVI NES configuration used in the subsequent comparison is selected from these recommended ranges. In this sense, Table 6 is not intended to prescribe a unique optimum, but to provide a practical parameter window within which satisfactory response reduction, reasonable stroke demand, and favorable robustness can be simultaneously achieved. This range-based interpretation is more consistent with the nonlinear and impact-assisted nature of the SSVI NES.

 doi:10.20944/preprints202605.1085.v1

4.3. Nominal Comparison Between the SSVI NES and the TMD

Having established the optimized TMD as the linear benchmark and identified a practical parameter window for the SSVI NES, this section compares the two devices under the nominal design condition. The representative SSVI NES configuration adopted in the following analysis is selected from the recommended parameter ranges summarized in Table 6, rather than from a single mathematically isolated optimum. In this way, the comparison reflects the practical operating region of the nonlinear impact absorber and provides a fair basis for assessing its nominal performance relative to the optimized TMD [4–8,14–21].

The comparison focuses on three aspects that are important for nacelle-mounted passive vibration mitigation: reduction of the nacelle fore-aft response, absorber motion demand, and supplementary interpretation of the associated dynamic behavior. The purpose is not to claim overwhelming superiority of the SSVI NES at the nominal design point, but to determine whether it can achieve vibration mitigation comparable to that of the optimized TMD while remaining more compatible with nacelle installation constraints [4,7,8,18,21–26].

4.3.1. Governing Equations of the SSVI NES

The SSVI NES is mounted inside the nacelle and arranged to act in the tower fore-aft direction. Relative to the TMD-controlled system, the SSVI NES introduces an additional nonlinear interaction force associated with unilateral impact between the oscillator and the single-sided barrier. In the present study, this interaction is described using a nonlinear viscoelastic impact model.

Accordingly, the controlled equation of motion of the primary structure can be written as

$$\mathrm{M\ddot{q} + C\dot{q} + Kq = F_w + F_{wa} + F_s + F_c e} \tag{22}$$

where $\mathrm{F_c}$ is the impact force generated by the SSVI NES and e is the location vector through which the force is transmitted to the nacelle degree of freedom.

The corresponding equation of motion of the SSVI NES oscillator is

$$m_n\ddot{x}_n + c_n\left(\dot{x}_n - \dot{x}_{\mathrm{top}}\right) + k_n\left(x_n - x_{\mathrm{top}}\right) = -F_c \tag{23}$$

where $\mathrm{m_n}$, $\mathrm{c_n}$, and $\mathrm{k_n}$ are the mass, damping, and nominal restoring stiffness of the SSVI NES, respectively, $\mathrm{x_n}$ is the displacement of the SSVI NES mass, and $\mathrm{x_{top}}$ is the nacelle fore-aft displacement.

The impact force is activated only when contact occurs. Defining the contact deformation as

$$\delta = x_n - x_{\mathrm{top}} - g_0 \tag{24}$$

where $\mathrm{g_0}$ is the initial gap between the SSVI NES mass and the impact barrier, the impact force is expressed as

$$F_c = \begin{cases} k_c\delta^{3/2} + c_{\mathrm{imp}}\dot{\delta}, & \delta > 0, \dot{\delta} > 0 \\ k_c\delta^{3/2}, & \delta > 0, \dot{\delta} \le 0 \\ 0, & \delta \le 0 \end{cases} \tag{25}$$

in which $\mathrm{k_c}$ is the contact stiffness and $\mathrm{c_{imp}}$ is the impact damping coefficient. In the Jankowski model, the damping term is active during the approach stage of impact, while the restoring contact force remains during the restitution stage. Under this formulation, the SSVI NES combines nonlinear restoring interaction and impact-induced dissipation, so that vibration reduction can be achieved through both nonlinear energy transfer and unilateral impact effects [22–26].

For the subsequent nominal comparison, the representative SSVI NES parameters are selected from the practical parameter ranges identified in Section 4.2. This treatment ensures that the comparison with the optimized TMD is based on a feasible and physically meaningful SSVI NES configuration rather than on an arbitrarily chosen parameter set.

 doi:10.20944/preprints202605.1085.v1

4.3.2. Representative SSVI NES Configuration

For the nominal-condition comparison, a representative SSVI NES configuration is selected from the practical parameter window identified in Section 4.2 and summarized in Table 6. The representative configuration is taken with an effective frequency ratio of $f_r = 0.9$,while the contact stiffness ratio and gap ratio are selected within the recommended moderate-to-high stiffness range and intermediate gap range, respectively. This choice is consistent with the parametric results, which show that satisfactory vibration mitigation and acceptable absorber motion demand can be achieved within a practical parameter region rather than at a single sharply defined optimum.

The purpose of selecting a representative SSVI NES configuration is not to prescribe a unique optimal design, but to provide a feasible and physically meaningful basis for comparison with the optimized TMD under the same nominal loading condition. In particular, the choice of $f_r = 0.9$ follows the combined response-and-stroke assessment presented in Section 4.2, where the engineering trade-off between nacelle response reduction and absorber motion demand is examined directly.

4.3.3. Response Comparison under the Nominal Condition

Under the nominal loading condition, the vibration-control performance of the representative SSVI NES is compared directly with that of the optimized TMD. The comparison is carried out using the performance metrics defined in Section 2.3, with particular emphasis on the nacelle fore-aft response and the corresponding absorber motion demand. The purpose of this comparison is to determine whether the SSVI NES can provide vibration mitigation comparable to that of the optimized linear benchmark while remaining more compatible with nacelle-mounted installation constraints.

Figure 13 presents the representative time-history responses under the nominal design condition. Compared with the uncontrolled case, both the optimized TMD and the representative SSVI NES reduce the nacelle fore-aft response effectively. At the exact design point, the optimized TMD may still provide slightly stronger local suppression, which is consistent with its parameter optimization under the prescribed objective function. Nevertheless, the response envelopes of the two controlled cases remain close to each other, indicating that the SSVI NES can achieve vibration mitigation comparable to that of the optimized TMD without relying on a sharply tuned linear resonance condition.

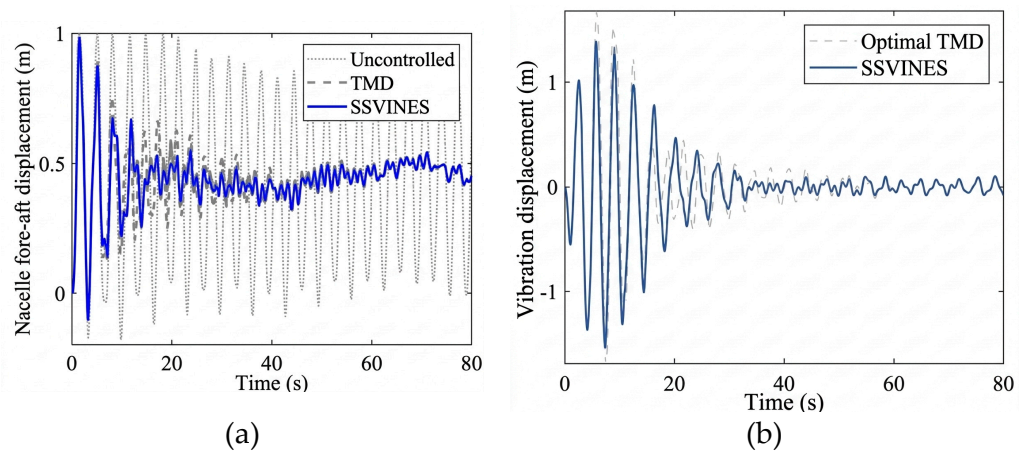

Figure 13. Time-history comparison under the design condition: (a) nacelle fore-aft displacement; (b) absorber displacement.

The motion of the attached absorbers is also compared in Figure 13b. The TMD response remains relatively regular and tuning-dominated, whereas the SSVI NES response exhibits a more irregular pattern associated with nonlinear interaction and unilateral impact. Under the same nominal

 doi:10.20944/preprints202605.1085.v1

condition, the maximum absorber displacement of the SSVI NES is significantly smaller than that of the TMD, while its control effectiveness remains comparable. This result is important for offshore wind turbine applications because it indicates that effective vibration mitigation can be achieved without requiring a large absorber stroke inside the nacelle.

Figure 14 compares the nacelle response in the frequency domain. Both devices suppress the dominant low-frequency response component effectively, confirming that the principal structural vibration mode is mitigated under the nominal condition. The TMD achieves this mainly through precise resonance tuning and viscous dissipation, whereas the SSVI NES relies on nonlinear restoring behavior combined with intermittent impact [22–26]. As a result, the SSVI NES does not exhibit overwhelming nominal superiority at the design point, but it does provide a similar level of response reduction through a more flexible nonlinear mitigation mechanism.

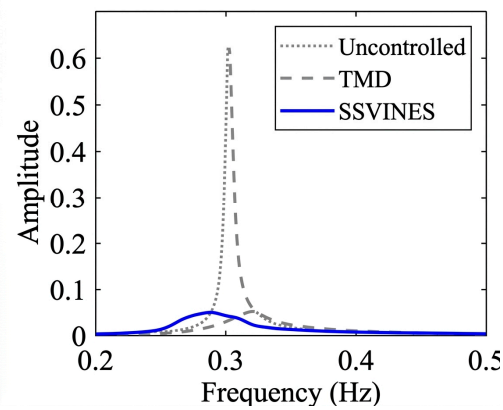

Figure 14. Frequency-domain comparison of nacelle fore-aft displacement under the nominal design condition.

Taken together, the nominal-condition comparison shows that the optimized TMD remains a strong linear benchmark passive controller at the design point, while the representative SSVI NES can achieve near-benchmark vibration mitigation with a smaller absorber motion demand. Therefore, under the nominal loading condition, the principal significance of the SSVI NES lies not in overwhelming nominal superiority, but in combining competitive control effectiveness with improved spatial compatibility for nacelle-integrated implementation.

4.4. Robustness under Frequency Detuning

Although the optimized TMD provides strong vibration suppression at the nominal design point, its effectiveness depends strongly on accurate tuning to the dominant structural frequency. In practical offshore wind turbine applications, however, the structural frequency may vary during service because of soil–structure interaction uncertainty, scour development, foundation flexibility, material degradation, changing operating states, and modeling errors [2,3,10–13]. Therefore, robustness under frequency detuning is an important criterion for assessing the practical applicability of nacelle-mounted passive vibration-control devices.

In this study, frequency detuning is introduced to examine whether the proposed SSVI NES can retain a more stable vibration-mitigation performance than the optimized TMD when the nominal tuning condition is no longer satisfied. The TMD represents a linear tuned absorber whose effectiveness is expected to decrease once the structural frequency deviates from the design value [4–8,14–21]. In contrast, the SSVI NES is expected to be less sensitive to such frequency variation because its control mechanism is governed by nonlinear energy transfer and impact-assisted dissipation rather than exact linear resonance tuning [22–26].

Figure 15 compares the cumulative dissipated energy of the optimized TMD, the detuned TMD, and the detuned SSVI NES.

 doi:10.20944/preprints202605.1085.v1

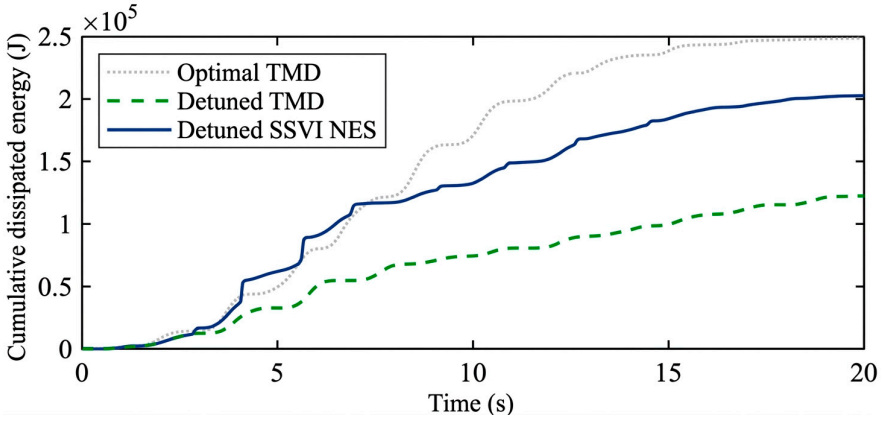

Figure 15. Cumulative dissipated energy of the optimized TMD, detuned TMD, and detuned SSVI NES under frequency detuning.

As shown in Figure 15, the optimized TMD exhibits the highest cumulative dissipated energy at the exact design point, which is consistent with its strong nominal control performance. However, once frequency detuning is introduced, the dissipated energy of the TMD decreases markedly. By contrast, the detuned SSVI NES retains a higher level of cumulative dissipated energy than the detuned TMD. This result indicates that the SSVI NES is less dependent on exact resonance matching and can continue to extract and dissipate vibration energy under off-design conditions through the combined effects of nonlinear restoring interaction and unilateral impact.

The degradation of control performance under detuning is further illustrated in Figure 16.

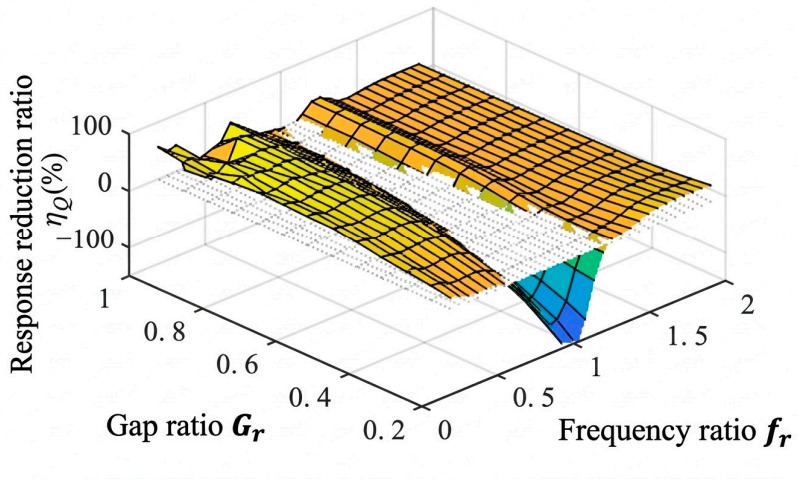

Figure 16. Response reduction ratio versus frequency detuning for the TMD and the SSVI NES under different gap ratios.

As shown in Figure 16, the TMD performs effectively only near the nominal tuning condition, and its response-reduction capability decreases rapidly as the frequency mismatch increases. This behavior reflects the narrow-band nature of linear tuned absorbers. In contrast, the SSVI NES maintains a more stable response-reduction capability over a broader detuning interval. Although its nominal performance does not necessarily exceed that of the optimized TMD, its control effectiveness deteriorates more gradually when the structural frequency shifts away from the design value. This retained effectiveness is particularly important for offshore wind turbines, whose dynamic characteristics may evolve during long-term service.

Representative time-history responses under a detuned condition are shown in Figure 17.

 doi:10.20944/preprints202605.1085.v1

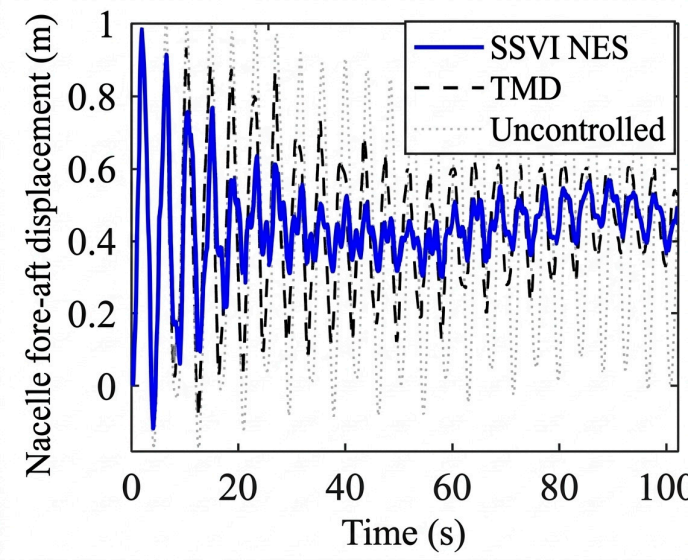

Figure 17. Representative nacelle fore-aft displacement responses under a detuned condition.

Figure 17 further confirms the different detuning sensitivities of the two control devices. When the TMD is substantially detuned, the nacelle fore-aft displacement increases noticeably, indicating that the advantage of precise linear tuning is largely lost. Under the same detuned condition, the SSVI NES still maintains effective reduction of the nacelle response. This behavior can be attributed to the broader nonlinear interaction mechanism of the SSVI NES. Unlike the TMD, which relies on a fixed tuning relationship between the absorber and the primary structure, the SSVI NES can exchange and dissipate energy through nonlinear interaction and impact activation over a wider frequency range.

Taken together, the detuning analysis shows that the optimized TMD remains highly effective near the nominal tuning point, whereas the SSVI NES retains a more stable level of vibration mitigation when frequency mismatch is introduced. From an engineering perspective, this retained effectiveness is the principal advantage of the SSVI NES for nacelle-mounted control of monopile offshore wind turbines, where exact tuning cannot always be guaranteed throughout the service life. Accordingly, the main value of the SSVI NES lies not in overwhelming superiority at the nominal design point, but in combining competitive nominal performance with improved robustness under off-design structural-frequency conditions.

5. Conclusions

This study investigated the vibration-control performance of a single-sided vibro-impact nonlinear energy sink (SSVI NES) for a monopile offshore wind turbine under representative wind, wave, and seismic loading conditions. A reduced-order coupled dynamic model was established based on the NREL 5 MW reference turbine, and the proposed SSVI NES was evaluated through comparison with an optimized tuned mass damper (TMD). The main conclusions are summarized as follows.

1. The reduced-order model provides an efficient and sufficiently accurate basis for control-oriented analysis of the monopile offshore wind turbine. The modal characteristics and baseline responses confirm that the dominant low-frequency structural dynamics are well captured. Under uncontrolled conditions, wind–wave loading results in sustained vibration, whereas seismic excitation introduces pronounced transient amplification and record-dependent variability.
2. The optimized TMD achieves strong vibration suppression under the nominal design condition and serves as a reliable linear benchmark passive controller. However, its effectiveness is concentrated within a relatively narrow tuning region, and its absorber stroke demand may

 doi:10.20944/preprints202605.1085.v1

increase depending on the selected mass ratio. This limitation is important for nacelle-mounted applications where installation space is inherently constrained.

3. The proposed SSVI NES exhibits a broader effective operating region in the nonlinear parameter space. The parametric analysis shows that satisfactory vibration mitigation and acceptable absorber motion demand can be achieved within a practical parameter window, rather than at a single sharply defined optimum. Under the nominal condition, the representative SSVI NES achieves nacelle fore-aft response reduction comparable to that of the optimized TMD while requiring a smaller absorber motion range, which is advantageous for nacelle-integrated implementation.
4. The principal advantage of the SSVI NES is observed under frequency-detuned conditions. While the performance of the TMD deteriorates rapidly once the structural frequency deviates from the nominal tuning point, the SSVI NES retains a more stable level of vibration mitigation through nonlinear interaction and unilateral impact. This reduced sensitivity to tuning uncertainty is particularly relevant for offshore wind turbines, where structural properties may vary over time.

Overall, the results indicate that the SSVI NES is a promising passive vibration-control solution for monopile offshore wind turbines, offering a balanced combination of comparable nominal performance, reduced absorber motion demand, and improved robustness under uncertain operating conditions. These characteristics contribute to enhanced structural serviceability and resilience of offshore energy infrastructure.

The conclusions should be interpreted within the scope of the present reduced-order model and the fore-aft control configuration considered herein. Future work should focus on higher-fidelity aero-hydro-servo-soil coupled modeling, multi-directional control strategies, systematic parameter optimization, and experimental validation.

Author Contributions: Methodology, A.A.; Software, G.Y.; Investigation, M.M.; Resources, X.Z.; Data curation, M.M.; Writing—original draft, M.M.; Writing—review & editing, Q.H.; Funding acquisition, G.Y. All authors have read and agreed to the published version of the manuscript.

Funding: This research was funded by Kashi University under grant number (2025) 2985.

Data Availability Statement: The original contributions presented in this study are included in the article. Further inquiries can be directed to the corresponding author.

Conflicts of Interest: The authors declare no conflict of interest.

References

1. Jonkman, J.; Butterfield, S.; Musial, W.; Scott, G. Definition of a 5-MW Reference Wind Turbine for Offshore System Development; NREL/TP-500-38060; National Renewable Energy Laboratory: Golden, CO, USA, 2009. https://doi.org/10.2172/947422
2. Sunday, K.M.; Brennan, F. A review of offshore wind monopiles structural design achievements and challenges. Ocean Eng. 2021, 235, 109409. https://doi.org/10.1016/j.oceaneng.2021.109409
3. Song, B.; Cummins, C.; Zou, Q. Coupled stability of offshore wind monopile foundations and submarine slopes under periodic loads. Appl. Ocean Res. 2023, 140, 103714. https://doi.org/10.1016/j.apor.2023.103714
4. Ghassempour, M.; Failla, G.; Arena, F. Vibration mitigation in offshore wind turbines via tuned mass damper. Eng. Struct. 2019, 183, 610–636. https://doi.org/10.1016/j.engstruct.2018.12.092
5. Dinh, V.N.; Basu, B. Passive control of floating offshore wind turbine nacelle and spar vibrations by multiple tuned mass dampers. Struct. Control Health Monit. 2015, 22, 152–176. https://doi.org/10.1002/stc.1666
6. Patro, S.R.; Panda, S.; Ramana, G.V.; Banerjee, A. Optimal multiple tuned mass dampers for monopile supported offshore wind turbines using Genetic Algorithm. Ocean Eng. 2024, 298, 117356. https://doi.org/10.1016/j.oceaneng.2024.117356

 doi:10.20944/preprints202605.1085.v1

7. Zhang, T.; Wang, W.; Li, X.; Wang, B. Vibration mitigation in offshore wind turbine under combined wind-wave-earthquake loads using the tuned mass damper inerter. Renew. Energy 2023, 216, 119050. https://doi.org/10.1016/j.renene.2023.119050
8. Zhang, W.; Zhao, H.; Bai, X.; Li, Y. Motion control of pentapod offshore wind turbines under earthquakes by tuned mass damper. J. Mar. Sci. Eng. 2019, 7, 224. https://doi.org/10.3390/jmse7070224
9. Ng, C.H. Seismic response of monopile-supported wind turbine systems: Combination laws for kinematic and inertial interaction. HKIE Trans. 2024, 31, 1–12. https://doi.org/10.33430/V31N4THIE-2024-0021
10. Carswell, W.; Arwade, S.R.; DeGroot, D.J. Soil-structure interaction effects in offshore wind support structures under monotonic, cyclic, and seismic loading. J. Offshore Mech. Arct. Eng. 2019, 141, 061903. https://doi.org/10.1115/1.4043505
11. Damgaard, M.; Ibsen, L.B.; Andersen, L.V.; Andersen, J.K. Model uncertainties for soil-structure interaction in offshore wind turbines. J. Mar. Sci. Eng. 2018, 6, 87. https://doi.org/10.3390/jmse6030087
12. Tirandazian, M.; Nouri, G. Effect of turbine weight on the seismic response of a wind turbine-monopile system located in liquefied multilayer soil. Shock Vib. 2021, 2021, 6622813. https://doi.org/10.1155/2021/6622813
13. Sahraeian, S.M.S.; Masoumi, M.A.; Najafgholipour, M.A.; Shafiee, A. Seismic response of monopile foundation of offshore wind turbines in liquefiable soils. Structures 2024, 64, 106591. https://doi.org/10.1016/j.istruc.2024.106591
14. Hussan, M.; Rahman, M.S.; Sharmin, F.; Kim, D.; Do, J. Multiple tuned mass damper for multi-mode vibration reduction of offshore wind turbine under seismic excitation. Ocean Eng. 2018, 160, 449–460. https://doi.org/10.1016/j.oceaneng.2018.04.041
15. Hussan, M.; Sharmin, F.; Kim, D. Multiple tuned mass damper based vibration mitigation of offshore wind turbine considering soil-structure interaction. China Ocean Eng. 2017, 31, 476–486. https://doi.org/10.1007/s13344-017-0054-x
16. Wang, S.; Liu, Y.; Zhang, H.; Li, X. Optimization study of a tuned mass damper for a large monopile wind turbine. Energies 2024, 17, 4460. https://doi.org/10.3390/en17174460
17. Ma, H.; Zhang, Y.; Liu, J.; Chen, X. Multi-degree-of-freedom tuned mass damper for vibration suppression of floating offshore wind turbine. J. Mar. Sci. Eng. 2026, 14, 634. https://doi.org/10.3390/jmse14070634
18. Li, X.; Zhang, Y.; Wang, J.; Chen, Z. Evaluation of tuned mass damper for offshore wind turbine using coupled fatigue analysis method. Energies 2025, 18, 4788. https://doi.org/10.3390/en18184788
19. Fathi, A.; Hollaway, D.; Kumar, R. Optimizing seismic performance of tuned mass dampers at various levels in reinforced concrete buildings. Buildings 2024, 14, 2443. https://doi.org/10.3390/buildings14082443
20. Wang, B.; Han, D.; Wang, W.; Li, X.; Shen, K.; Li, Y. Modeling and optimization of multiple tuned mass dampers for a barge-type floating offshore wind turbine. Front. Mar. Sci. 2022, 9, 994848. https://doi.org/10.3389/fmars.2022.994848
21. Zhang, H.; Xu, Y.; Li, Y.; Wang, C. Application of an eddy current-tuned mass damper to vibration mitigation of offshore wind turbines under windstorm and typhoon conditions. Energies 2018, 11, 3319. https://doi.org/10.3390/en11123319
22. Vakakis, A.F.; Gendelman, O.V.; Bergman, L.A.; Mojahed, A.; Gzal, M. Nonlinear targeted energy transfer: State of the art and new perspectives. Nonlinear Dyn. 2022, 108, 711–741. https://doi.org/10.1007/s11071-022-07216-w
23. Gendelman, O.V.; Manevitch, L.I.; Vakakis, A.F.; M'Closkey, R. Energy pumping in nonlinear mechanical oscillators: Part I—Dynamics of the underlying Hamiltonian systems. J. Appl. Mech. 2001, 68, 34–41. https://doi.org/10.1115/1.1345524
24. AL-Shudeifat, M.A.; Wierschem, N.; Quinn, D.D.; Vakakis, A.F.; Bergman, L.A.; Spencer, B.F., Jr. Numerical and experimental investigation of a highly effective single-sided vibro-impact nonlinear energy sink for shock mitigation. Int. J. Non-Linear Mech. 2013, 52, 96–109. https://doi.org/10.1016/j.ijnonlinmec.2013.02.004
25. AL-Shudeifat, M.A. Highly efficient nonlinear energy sink. Nonlinear Dyn. 2014, 76, 1905–1920. https://doi.org/10.1007/s11071-014-1256-x

 doi:10.20944/preprints202605.1085.v1

26. Wu, Z.; Paredes, M.; Seguy, S. Targeted energy transfer in a vibro-impact cubic NES: Description of regimes and optimal design. J. Sound Vib. 2023, 545, 117425. https://doi.org/10.1016/j.jsv.2022.117425
27. IEC. IEC 61400-3-1:2019 Wind Energy Generation Systems—Part 3-1: Design Requirements for Fixed Offshore Wind Turbines; International Electrotechnical Commission: Geneva, Switzerland, 2019.
28. Kaimal, J.C.; Wyngaard, J.C.; Izumi, Y.; Coté, O.R. Spectral characteristics of surface-layer turbulence. Q. J. R. Meteorol. Soc. 1972, 98, 563–589. https://doi.org/10.1002/qj.49709841707
29. Morison, J.R.; Johnson, J.W.; Schaaf, S.A. The force exerted by surface waves on piles. J. Pet. Technol. 1950, 2, 149–154. https://doi.org/10.2118/950149-G
30. Hasselmann, K.; Barnett, T.P.; Bouws, E.; Carlson, H.; Cartwright, D.E.; Enke, K.; et al. Measurements of Wind-Wave Growth and Swell Decay during the Joint North Sea Wave Project (JONSWAP); Deutsche Hydrographische Zeitschrift, Reihe A, No. 12, 1973.
31. Jonkman, B.J. TurbSim User's Guide: Version 1.50; NREL/TP-500-46198; National Renewable Energy Laboratory: Golden, CO, USA, 2009. https://doi.org/10.2172/965520
32. Ancheta, T.D.; Darragh, R.B.; Stewart, J.P.; Seyhan, E.; Silva, W.J.; Chiou, B.S.-J.; et al. NGA-West2 database. Earthq. Spectra 2014, 30, 989–1005. https://doi.org/10.1193/070913EQS197M
33. Moriarty, P.J.; Hansen, A.C. AeroDyn Theory Manual; NREL/TP-500-36881; National Renewable Energy Laboratory: Golden, CO, USA, 2005. https://doi.org/10.2172/15014831
34. Ning, A. Development and validation of a new blade element momentum skewed-wake model within AeroDyn. In Proceedings of the 33rd ASME Wind Energy Symposium; National Harbor, MD, USA, 5–9 January 2015.
35. Buhl, M.L., Jr. New Empirical Relationship between Thrust Coefficient and Induction Factor for the Turbulent Windmill State; NREL/TP-500-36834; National Renewable Energy Laboratory: Golden, CO, USA, 2005.
36. OpenFAST Developers. OpenFAST Documentation; National Renewable Energy Laboratory: Golden, CO, USA. Available online: https://openfast.readthedocs.io/ (accessed on 15 April 2026).